THE EMBO JOURNAL

Mechanism of endophilin N-BAR domain-mediated membrane curvature

Jennifer L Gallop[1,3,4], Christine C Jao[2,3], Helen M Kent[1], P Jonathan G Butler[1], Philip R Evans[1,*], Ralf Langen[2,*] and Harvey T McMahon[1,*]

[1]MRC Laboratory of Molecular Biology, Cambridge, UK and [2]Department of Biochemistry and Molecular Biology, Zilkha Neurogenetic Institute, University of Southern California, Los Angeles, CA, USA

Endophilin-A1 is a BAR domain-containing protein enriched at synapses and is implicated in synaptic vesicle endocytosis. It binds to dynamin and synaptojanin via a C-terminal SH3 domain. We examine the mechanism by which the BAR domain and an N-terminal amphipathic helix, which folds upon membrane binding, work as a functional unit (the N-BAR domain) to promote dimerisation and membrane curvature generation. By electron paramagnetic resonance spectroscopy, we show that this amphipathic helix is peripherally bound in the plane of the membrane, with the midpoint of insertion aligned with the phosphate level of headgroups. This places the helix in an optimal position to effect membrane curvature generation. We solved the crystal structure of rat endophilin-A1 BAR domain and examined a distinctive insert protruding from the membrane interaction face. This insert is predicted to form an additional amphipathic helix and is important for curvature generation. Its presence defines an endophilin/nadrin subclass of BAR domains. We propose that N-BAR domains function as low-affinity dimers regulating binding partner recruitment to areas of high membrane curvature.

Introduction

Endophilin A proteins have been implicated in membrane curvature generation in synapses during clathrin-mediated endocytosis as they bind to the endocytic proteins dynamin and synaptojanin. In *Drosophila* and in *Caenorhabditis elegans*, endophilin mutants have defective synaptic vesicle recycling (Guichet *et al*, 2002; Rikhy *et al*, 2002; Verstreken *et al*, 2002; Schuske *et al*, 2003). In higher organisms, overexpression of the endophilin SH3 domain, antibodies against endophilin and peptides that bind to the SH3 domain all result in the inhibition of vesicle recycling and the accumulation of clathrin-coated profiles, suggesting an involvement in clathrin-coated vesicle formation (Ringstad *et al*, 1999; Simpson *et al*, 1999; Gad *et al*, 2000). There is still some vesicle endocytosis in endophilin-deficient flies, and the slower kinetics of this residual component is consistent with clathrin-mediated endocytosis (Dickman *et al*, 2005). Thus, endophilin must either speed up a clathrin-mediated pathway in flies or be involved in a separate, clathrin-independent endocytic pathway that is faster than clathrin-dependent endocytosis.

The ability to effect membrane curvature may implicate endophilin in early stages of vesicle formation where it could help to generate the initial membrane curvature, or in late stages where it could aid in vesicle neck formation. The stage of action has been examined in the context of clathrin-coated vesicle formation given that clathrin-coated profiles are easily observed by electron microscopy. Evidence against an early stage function for endophilin comes from studies on clathrin-coated vesicle formation in a cell-free assay. Here depletion of endophilin did not affect the number and morphology of clathrin-coated pits (Ringstad *et al*, 1999). A lipid-modifying activity of endophilin to aid in membrane curvature has also been excluded (Gallop *et al*, 2005). Evidence for late stage involvement has been obtained from this same cell-free coating assay where a significant reduction of dynamin-coated structures following endophilin depletion was observed. Thus, endophilin could be involved in late stages of endocytosis through its recruitment of dynamin and/or the lipid phosphatase synaptojanin. PtdIns(4,5)P$_2$ is an important lipid in anchoring a number of clathrin-coated vesicle components to the membrane, including the clathrin recruitment and polymerising protein AP180 (Ford *et al*, 2001), and thus depletion of this lipid by the mobilisation of synaptojanin to coated vesicles would help release the coat components. Indeed, endophilin is required in *C. elegans* for the recruitment of synaptojanin to nerve terminals (Schuske *et al*, 2003), and deletion of synaptojanin in mice leads to an accumulation of coated vesicle profiles (Cremona *et al*, 1999). In the lamprey reticulospinal synapse, disruption of the endophilin SH3 domain interactions perturbs uncoating of clathrin-coated vesicles (Gad *et al*, 2000). Defective vesicle scission in this study also points to a role in dynamin recruitment. We should note however that there is no firm biochemical assignment of endophilin to clathrin-mediated endocytosis, as endophilin does not enrich in clathrin-coated vesicles nor bind to specific components of the clathrin-coat machinery, and the phenotypes observed could well be indirect.

*Corresponding authors. HT McMahon, MRC Laboratory of Molecular Biology, Hills Road, Cambridge CB2 2QH, UK. Tel.: +44 1223 402311; Fax: +44 1223 402310; E-mail: hmm@mrc-lmb.cam.ac.uk or R Langen, Department of Biochemistry and Molecular Biology, Zilkha Neurogenetic Institute, University of Southern California, 1501 San Pablo Street, Los Angeles, CA 90033, USA. E-mail: langen@usc.edu or PR Evans, MRC Laboratory of Molecular Biology, Hills Road, Cambridge CB2 2QH, UK. E-mail: pre@mrc-lmb.cam.ac.uk
[3]These authors contributed equally to this work
[4]Present address: Department of Systems Biology, Harvard Medical School, Boston, MA 02115, USA

By sequence analysis, there are A and B subfamilies of endophilins. In the A subfamily, there are endophilins A1 (also called endophilin1, SH3P4, SH3GL2 and EEN-B1), A2 (also called endophilin2, SH3P8 and SH3GL1) and A3 (also called endophilin3, SH3P13 and SH3GL3) and in the B subfamily there are endophilins B1 (also called SH3GLB1) and B2 (also called Bif1, SH3GLB2 and EEN). Some of these are synaptically enriched, whereas others are more ubiquitously expressed (for review see Huttner and Schmidt, 2000). They all have the same overall domain structure, with an N-terminal N-BAR domain (BAR domain with an additional predicted N-terminal amphipathic helix) coupled to an SH3 domain by a variable linker region. The ubiquitous distribution of some endophilins, their interactions with membranes and trafficking proteins, and the role of endophilin-A1 in synaptic vesicle endocytosis support the hypothesis that endophilins perform a general function in forming transport carriers in different trafficking pathways. A homologous protein, amphiphysin, has a similar overall domain structure (with an N-BAR domain followed by an SH3 domain; see Figure 1A for scheme) and is implicated in T-tubule formation in muscle and in clathrin-coated vesicle formation (Bauerfeind *et al*, 1997; Razzaq *et al*, 2001; Lee *et al*, 2002; Evergren *et al*, 2004).

The deformation of membrane that is required to make small-diameter transport vesicles, as found at synapses, has a significant energetic requirement. When making small liposomes *in vitro*, this energy is provided by intense sonication. *In vivo*, high curvature can be achieved using peripheral membrane binding proteins that effect and stabilise curvature (for review see McMahon and Gallop, 2005). In particular, the insertion of amphipathic helices into the hydrophobic phase of the bilayer is proposed to be a general biophysical mechanism for curvature generation during vesicle budding, based on point mutagenesis in amphiphysin (Peter *et al*, 2004), endophilin (Farsad *et al*, 2001), epsin (Ford *et al*, 2002) and Sar1 GTPase (Lee *et al*, 2005). Until now, insertion of amphipathic helices for vesicle budding proteins has not been shown directly. Here we show, using electron paramagnetic resonance spectroscopy (EPR), that the N-terminal amphi-
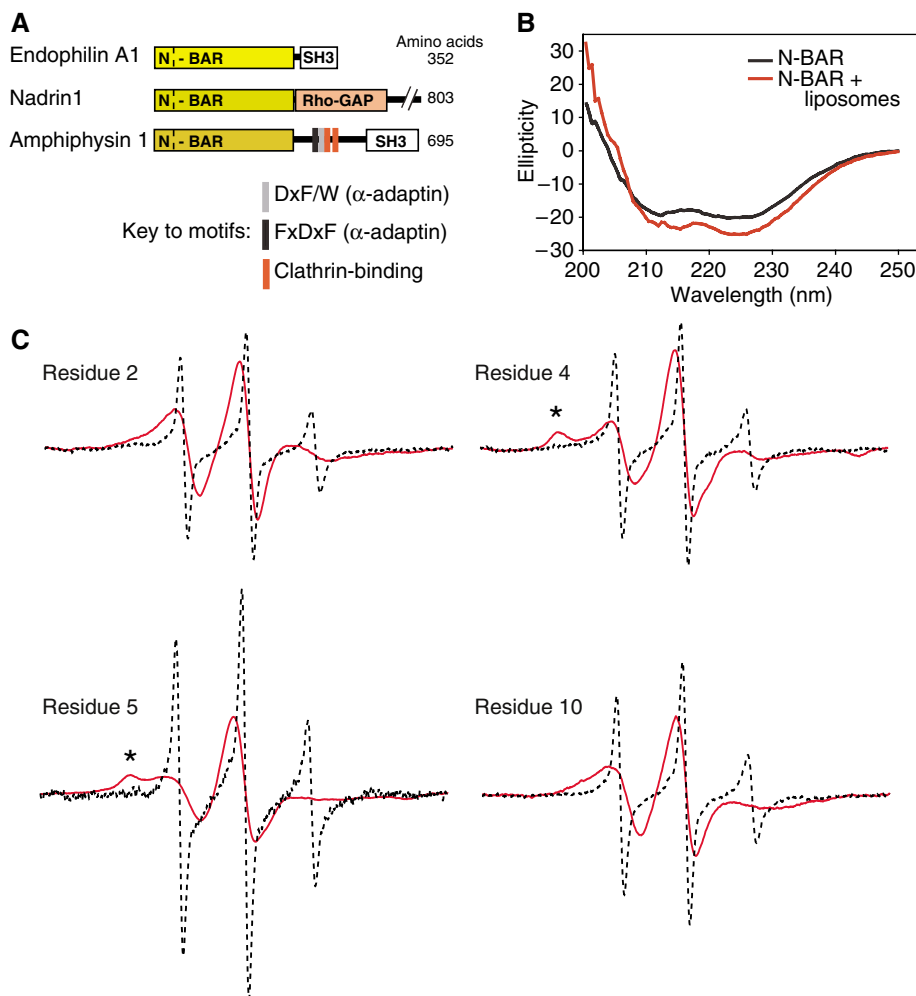

Figure 1 Ordering of N-terminal residues of endophilin on membrane binding. (**A**) Domain structure of endophilin, nadrin and amphiphysin. The C-terminal region of nadrin has been truncated. (**B**) In the CD spectrum (room temperature), there is additional α-helical structure in the N-BAR domain on incubation with 50 nm Folch liposomes. This was not seen for the BAR alone (not shown). (**C**) EPR spectra of endophilin A1 N-BAR domains in the absence (black dash) and presence (red) of liposomes. Sample traces for residues 2, 4, 5 and 10 are shown. Other traces are shown in Supplementary Figure 1. Asterisks point to additional immobilisation compared to surrounding residues on membrane binding. Protein (2 μM) was incubated with 1.4 mg/ml liposomes and centrifuged to separate bound from unbound. Membrane-bound spectra are shown at a magnification of 2.5.

pathic helix of endophilin inserts into membranes and we elucidate the orientation and depth of helix penetration. In the case of N-BAR domains, both their amphipathic helices and BAR domains have been implicated in the promotion of membrane curvature, and the relative importance of these two modules has been unclear. *In vitro*, the N-BAR domain of endophilin tubulates liposomes and a truncation that includes approximately half the BAR domain is also effective, as are isolated BAR domains (Farsad *et al*, 2001; Peter *et al*, 2004). We now carry out a thorough analysis of the endophilin N-BAR domain using crystallographic and biophysical techniques. The principles uncovered (driving of curvature by amphipathic helices and selection or limiting of membrane curvature by a BAR domain, and the feed-forward behaviour of N-BAR domain binding) will also apply to other proteins where one finds this same combination of amphipathic helix followed by BAR domain, including nadrin/RICH and BRAP1/Bin2 N-BAR domains. By homology screening, we also find that nadrin and endophilin are in the same structural subclass of BAR domain owing to an insert present on the concave face. This insert includes a further predicted amphipathic helix that exhibits membrane interaction capability. Our measurements of the behaviour of amphipathic helices on membranes are also likely true for the epsin family of proteins and also for the Arf, Arl and Sar family GTPases.

Results

An N-terminal amphipathic helix of endophilin folds and inserts into membranes

Predicted N-terminal amphipathic helices have been proposed to fold on membrane binding and anchor membrane curvature-generating proteins in the membrane to cause displacement of lipids in one leaflet, promoting curvature generation (Ford *et al*, 2002; Peter *et al*, 2004). We now use direct biophysical methods to determine the structure of these residues on membrane binding.

On liposome binding, there is an increase in α-helicity of the N-BAR domain of endophilin from 36 to 48% (estimated from circular dichroism; see Figure 1B), which is not observed in the absence of the N-terminal residues (not shown), implying the formation of additional helical structures. To test how the predicted N-terminal amphipathic helix folds, whether it inserts into membranes and to determine its topology in relation to the membrane, we used EPR together with site-directed spin labelling. A series of N-BAR domains were made where cysteines were substituted for each residue from 2 to 16 by site-directed mutagenesis. Spin labels were then attached to each cysteine mutant and the protein was used for EPR analysis. The EPR spectra of the spin-labelled derivatives in solution are very sharp, and on membrane binding these are broadened for each residue. These data show that this N-terminal region is disordered in solution and becomes ordered upon membrane binding (see example spectra in Figure 1C and the full range in Supplementary Figure 1). Residues 4, 5, 8 and 16, which are predicted to lie on a single plane of the predicted amphipathic helix, also show additional immobilisation (see asterisks in Figure 1C). This may indicate some other interactions with the BAR domain or lipid headgroups.

The accessibility of each spin-labelled site to oxygen (which preferentially partitions into membranes) and to

NiEDDA (preferentially in solution) is plotted in Figure 2A and shows which residues penetrate the bilayer. Up to residue 16, the O_2 and NiEDDA accessibilities ($\Pi(O_2)$ and $\Pi(\text{NiEDDA})$) exhibit a periodicity of 3–4 amino acids, consistent with the formation of a continuous α-helical structure. Importantly, the periodicities of access to the respective colliders are 180° out of phase. Such behaviour is typical for asymmetrically solvated α-helices in which one face is exposed to the membrane where the accessibility to O_2 is high; in contrast, residues on the opposing face are solvent-exposed and consequently more accessible to the hydrophilic
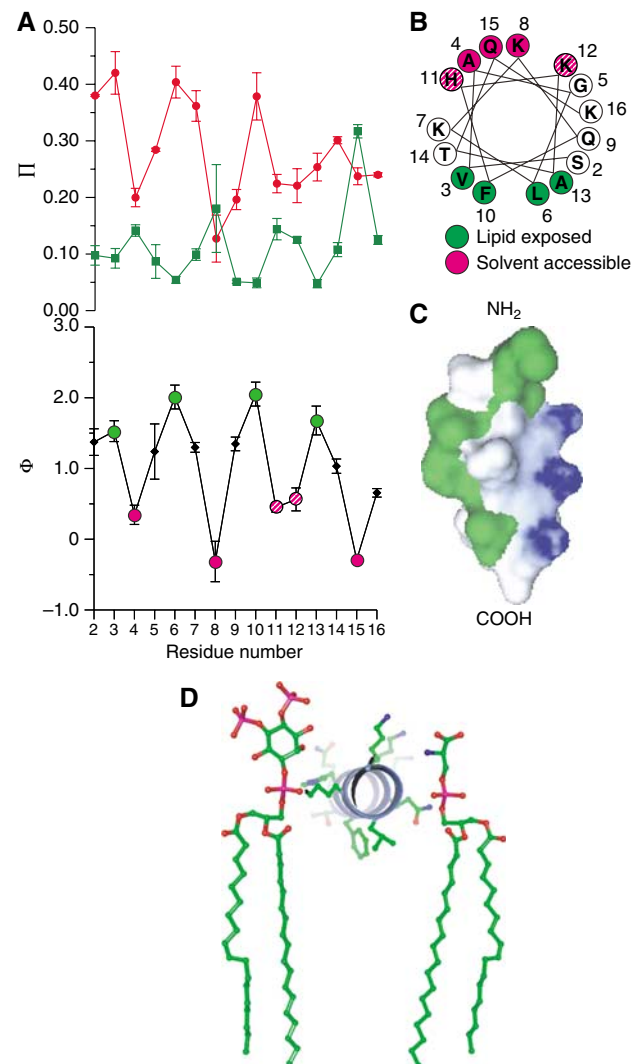

Figure 2 Membrane insertion and orientation of endophilin N-terminal amphipathic helix. (**A**) Oxygen (red circles) and NiEDDA (green squares) accessibilities (Π) of membrane-bound N-BAR domain as a function of label position. The graph below shows a $\ln(\Pi$ ratio) plot (Φ) showing the differential access of colliders to the spin label and the penetration of hydrophobic residues into the membrane. The periodic oscillation is indicative of a helical structure. Equivalent maxima indicate that the helix lies planar to the membrane. (**B**) Helical wheel representation showing hydrophobic and charged faces. (**C**) Model of the amphipathic helix, residues 1–16 with hydrophobic residues coloured green and surface charge potential also shown. (**D**) Model of the N-BAR amphipathic helix to scale with PtdIns(4,5)P_2 and PtdSer lipids showing the depth of penetration of the helix as calculated from data in (A) and penetration measurements, described in Materials and methods.

NiEDDA. The membrane exposure of a given site can be conveniently summarised by the contrast parameter $\Phi = \ln(\Pi(O_2)/\Pi(\text{NiEDDA}))$, which is proportional to the depth of membrane immersion (Altenbach *et al*, 1994). As shown in Figure 2B and C, membrane-exposed residues, corresponding to local maxima of Φ, cluster on one side of the helical wheel, whereas solvent-exposed sites (local minima of Φ) lie on the opposite face. The polar, more solvent-exposed residues of the helix have considerable positive charge and will prefer negatively charged lipid headgroups or a negative patch on an adjacent protein. The immersion depths of the lipid-facing residues were calibrated using labelled hydrocarbon chains (Altenbach *et al*, 1994) (see Materials and methods). Based on this calibration and the data in Figure 2A, we can place the centre of the helix near the phosphate level (Figure 2D). This is the first direct demonstration of amphipathic helix membrane insertion for an endocytic protein and we propose that this will apply to all N-BAR proteins, epsin family members and Arf/Arl/Sar proteins, thus providing a potential general mechanism by which membrane curvature is generated by these classes of proteins.

BAR domain structure

The N-terminal amphipathic helix of endophilin is followed immediately by a predicted BAR domain, which is expected to sense or stabilise positive membrane curvature (Peter *et al*, 2004). As the sequence homology between the endophilin and amphiphysin BAR domains (where a structure was already available) is low, we crystallised rat endophilin BAR to elucidate the curvature of the domain (Figure 3A and Supplementary Figure 2). A similar structure of mouse endophilin BAR domain has since been published (Weissenhorn, 2005) and when these are overlaid the r.m.s. deviation on the dimer is 0.95 Å for 392/408 residues. Structural details are marked on the endophilin sequence in Figure 4 and the N-terminal amphipathic helix is labelled as helix zero (after the epsin ENTH nomenclature; Ford *et al*, 2002) given that it folds on membrane binding (Figure 2A) despite being invisible in the unliganded crystal structure. The surface charge distribution of endophilin is similar to that of amphiphysin but more negative charges are concentrated on the convex face (see endophilin in Figure 3C and amphiphysin in Figure 3D). The high negative charge on the convex surface is conserved among endophilins (Supplementary Figure 2). In the structure solved by Weissenhorn, 11 cadmium ions were bound to the surface and he posits that these may mimic calcium binding sites of endophilin *in vivo*. We looked for calcium binding using di-bromo BAPTA, which allows detection of low micromolar affinities, and by using isothermal titration calorimetry, which allows detection of nanomolar affinity interactions (Figure 3F and G). We see no evidence of specific calcium interactions.

The curvature of endophilin BAR, formed by the angle of dimerisation and kinks in its helices, is very close to that of amphiphysin BAR (see overlay in Figure 3B and structural alignment in Figure 4) and arfaptin BAR (not shown), and thus these proteins cannot be distinguished by a difference in their predicted membrane curvature preference. A large hydrophobic patch is buried in the dimer interface (coloured green on the surface-represented monomer in Figure 3E). The

buried surface area is 2870 Å^2 per monomer, whereas in amphiphysin only 2400 Å^2 is buried. The curvature of the domain is likely to be rigid, as the mouse and the rat endophilin BAR structures are derived from crystals with completely different crystal packing, yet these structures superimpose closely and show the same radius of curvature (85 Å in the absence of the helix1 insert; Figure 3E; see next paragraph). In the present structure of the rat endophilin BAR, the extremities are involved in crystal contacts, leading to ordering of these flexible regions.

Endophilin BAR has an extra insert in the middle of its membrane binding face as compared to amphiphysin BAR. We call this the 'helix1 insert' (H1I, residues 60–87). The sequence of this insert differs considerably between endophilins and is also found in nadrin N-BAR family members. The QPNP sequence, which follows the break in helix1, appears to be diagnostic for endophilin family members across different species (Supplementary Figure 2). The H1I is mostly invisible (and thus disordered) in the crystal structure (Figure 2A) apart from an initial short helix (see Figure 4). This is predicted to continue as an amphipathic helix for several more turns. This would be particularly favoured in the low dielectric constant environment under the BAR domain and near the membrane. In a helical wheel representation (see Figure 3H), the hydrophobic side of the predicted helix is flanked on both sides by positively charged residues. This may indicate penetration of the membrane by the hydrophobic residues (similar to the N-terminal amphipathic helix) with accompanying electrostatic interactions with the charged lipid headgroups. Although by circular dichroism we were unable to detect an increase in helicity upon addition of liposomes to the BAR domain, this is not surprising as the BAR domain alone does not bind well to membranes and at least part of the helix appears to be already folded before binding. We chose one residue beyond the initial helix (M70) to test the possibility of folding on membrane interaction. The EPR spectrum shows some ordering of this residue upon membrane interaction (Figure 3I). It should be noted, however, that the spectral change upon membrane interaction is not as pronounced as in the N-terminal regions. This is owing to the fact that, in solution, position 70 is less dynamic than the N-terminal residues and consequently the observed mobility changes are less dramatic. This is also not surprising given that this helix appears to start to fold in the crystal structure. The O_2 and NiEDDA accessibilities for residue 70 resulted in a Φ value of 1.5, demonstrating that this position is indeed membrane-exposed at an immersion depth of approximately 6 Å. A predicted amphipathic sequence is also found at the C-terminal end of the nadrin insert.

We find no evidence in our structure for a lysophosphatidic acid acyl transferase active site. We have previously tested extensively for biochemical evidence of this activity and showed that it was a contamination of protein preparation (Gallop *et al*, 2005).

To test if the dimerisation seen in the crystal holds true in solution, we used equilibrium ultracentrifugation of the N-BAR domain (Figure 5A and residuals plotted in Figure 5B) and full-length protein (Supplementary Figure 4A). The dimerisation constant for the N-BAR is 10 μM and fits very well to a monomer:dimer equilibrium. This means that the protein could well be monomeric in cells—the concentration of
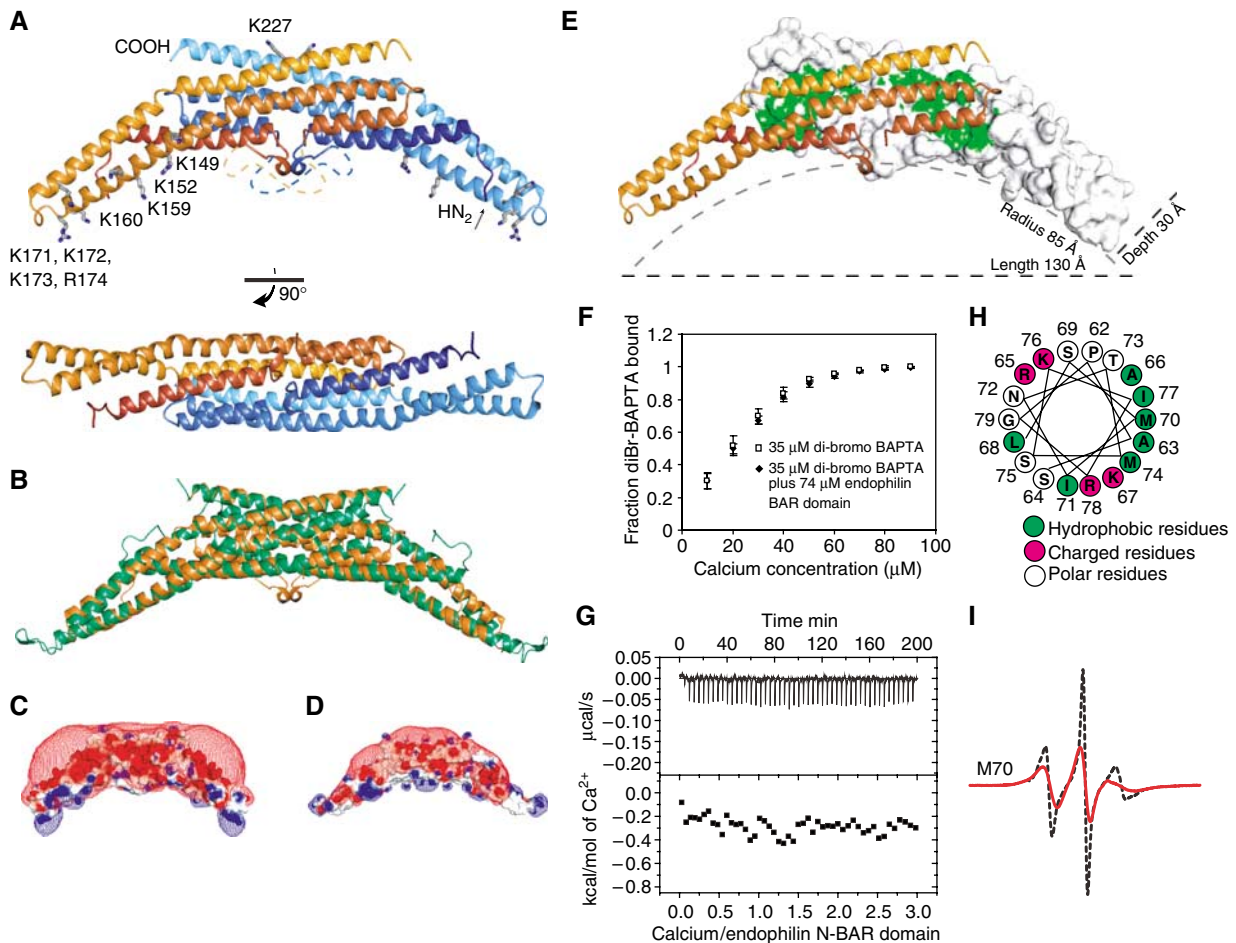
Figure 3 Endophilin N-BAR crystal structure. (**A**) Ribbon diagram of the banana-shaped rat endophilin-A1 BAR domain (Protein Data Bank (PDB) accession number 2c08) with a view of the concave surface below. Monomers are dark to light from NH_2- to COOH-termini with one coloured in brown to yellow and the other in dark blue to light blue. Lysine and arginine residues potentially important for membrane binding and K227 used to examine dimerisation are marked. (**B**) Superposition of the endophilin BAR domain (orange) with amphiphysin BAR (green). (**C**) Surface representation of the BAR domain of endophilin coloured according to electrostatic potential and a mesh equipotential surface contoured at 0.05 V. (**D**) Similar representation for amphiphysin as in (**C**). Both molecules are negatively charged (red) except on the concave face and the tips of the crescent, which are positively charged (blue). The overall shapes are very similar. (**E**) Hydrophobic residues in the dimer interface of rat endophilin-A1 BAR are coloured green on the surface-represented monomer. Dimensions of the BAR domain are also indicated. (**F**) Calcium does not bind to the endophilin N-BAR domain. The endophilin N-BAR domain was decalcified by purification in the presence of 2 mM EDTA followed by incubation with 10 mM EDTA and then extensive dialysis against Ca-free buffer (prepared using plastics). The absorbance of di-bromo BAPTA (affinity for Ca^{2+} of 2 μM in the absence of Mg^{2+}) at 265 nm was followed on calcium titration in the presence and absence of decalcified endophilin BAR domain. No difference was observed, suggesting that endophilin does not effectively compete with di-bromo BAPTA, even at double the concentration, for Ca^{2+} ions. (**G**) Isothermal titration calorimetry was used to test for heat changes on $CaCl_2$ injection into decalcified endophilin N-BAR domain. These experiments were performed with 6 μl injections of 1 mM $CaCl_2$ into 45 μM full-length endophilin and 76 μM endophilin N-BAR domain at 10 or 25°C. Example results for the N-BAR domain are shown and no binding was observed. (**H**) Modelling of helix1 insert residues 62–79 as an α-helix. Hydrophobic residues are predominantly on one side and are flanked by positively charged residues. The remaining residues on this insert are not predicted to form an amphipathic helix. (**I**) EPR spectra of N-BAR M70C in the absence (black dash) and presence (red) of liposomes. The red spectrum is magnified by 2.5.

endophilin in brain extract was estimated by blotting to be ∼0.1 μM, making the concentration at the synapse at perhaps ∼1 μM. For the full-length protein, there is evidence of higher order oligomers at high concentrations (Supplementary Figure 4A). This could be due to the previously proposed intramolecular interaction between the SH3 domain and the central proline-rich linker region (Chen *et al*, 2003).

As the model for curvature sensing by BAR domains is binding via the concave face (Peter *et al*, 2004) and the concave nature is only found in the dimeric form, it is surprising that the K_D for dimerisation in solution is as high as 10 μM (Figure 5A). Spin coupling between labelled site-directed cysteine mutants at position 227 was used to test if

the dimer is the predominant form of the protein on membranes. K227 is located near the dimerisation interface, and the α-carbon distance between the two K227 residues in the crystal dimer is 8 Å (see residue marked in Figure 3A). Introduction of a spin label at position 227 gave rise to a strong spin–spin interaction for this endophilin mutant and the resulting spectrum of the membrane-bound form exhibited strong dipolar broadening that is characteristic for spin labels in close proximity (Figure 5C, red trace). This spectrum was very different from a control spectrum for the K227 derivative, in which the dipolar interaction was strongly reduced by co-mixing of 25% labelled protein with 75% unlabelled protein (Figure 5C, black trace). Quantitative
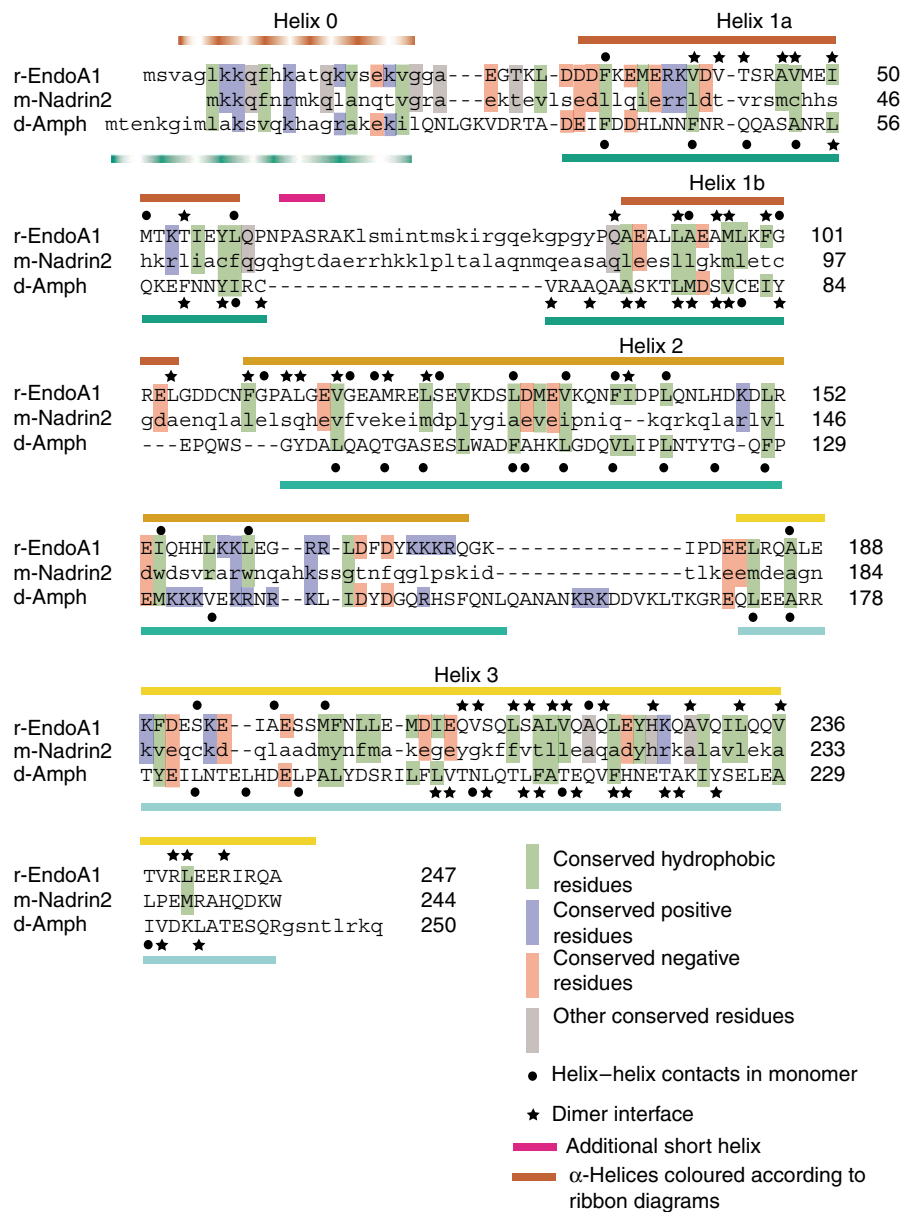
Figure 4 Structure-based sequence alignment of endophilin and amphiphysin BAR domains and alignment to nadrin showing close homology to endophilin.

analysis of the spectra with and without dipolar interaction allowed us to determine inter-spin label distances using Pake patterns (Rabenstein and Shin, 1995; Altenbach *et al*, 2001) and the resulting distances ranged from ∼8 to 10 Å (Figure 5D). These data are in excellent agreement with the distance between these labels predicted from the crystal structure and clearly demonstrate that membrane-bound endophilin forms the dimer interactions seen in the crystal.

Amphipathic helices and the BAR domain of endophilin collaborate to effect membrane curvature

The ability of endophilin to generate and stabilise membrane curvature can be assessed using liposomes rich in negatively charged lipids to which the N-BAR domain binds. By electron microscopy, we can determine the shape changes of these liposomes. The amphiphysin N-BAR domain and the arfaptin2 BAR domain constrict liposomes into tubules and higher

concentrations of the BAR domain proteins lead to vesiculation (Peter *et al*, 2004). Here, tubulation is the initial response of the liposome owing to an increase in curvature in one direction being compensated by a relaxation in a perpendicular direction.

The endophilin N-BAR domain has three major functional components: the N-terminal amphipathic helix, the BAR domain and an internal amphipathic helix (H1I) in a loop insert. We made a series of mutants to examine their contribution to membrane binding and curvature generation (Figure 6). Wild-type (WT) N-BAR (and full-length protein) forms highly curved tubules (of 35–50 nm diameter) from liposomes, and at high concentrations of protein many small vesicles (35–50 nm diameter) are also formed.

Mutation of F10 in the endophilin N-BAR domain (on the hydrophobic face of the N-terminal amphipathic helix) or deletion of the amphipathic helix leaving just the BAR
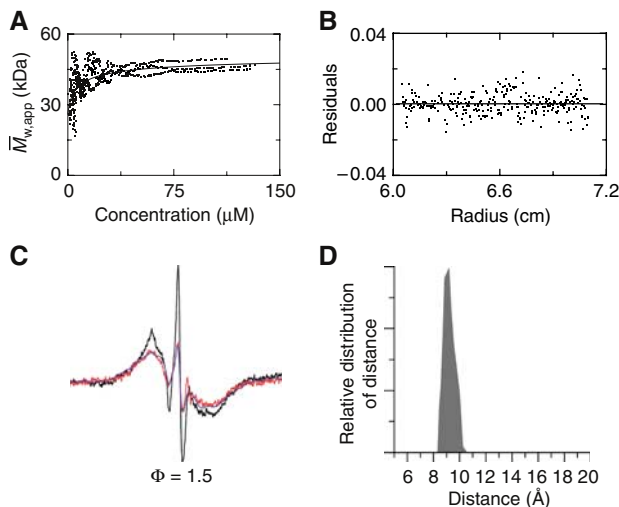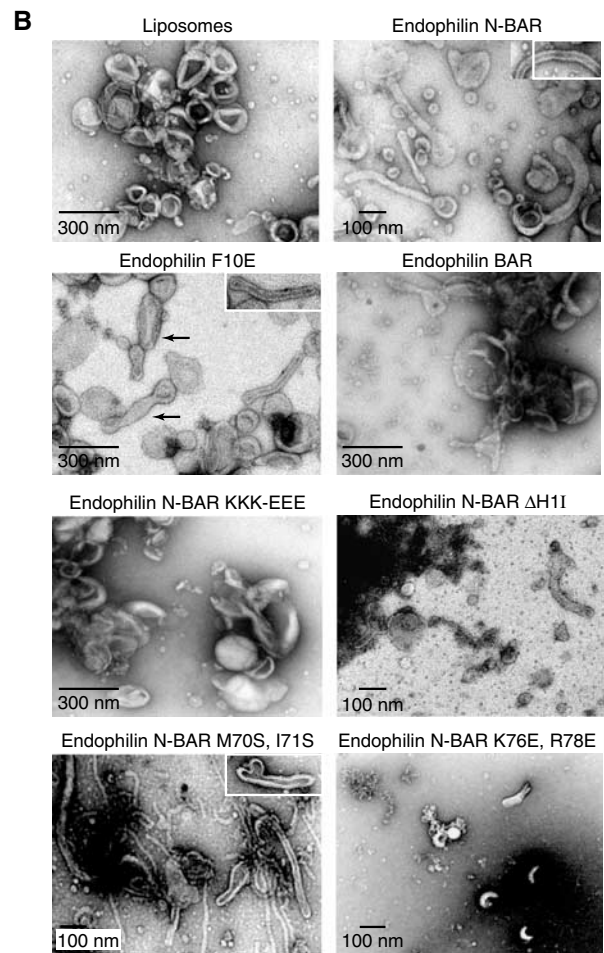
Figure 5 Endophilin N-BAR dimerisation on membrane binding. (**A**) Equilibrium sedimentation data for rat endophilin-A1 N-BAR domain. Endophilin N-BAR domain dimerises with a K_d of $\sim 10\,\mu M$. The readings from three cells are fitted with an ideal monomer/dimer equilibrium that fits with a 26 kDa monomer. The calculated molecular mass is 28.7 kDa. Residuals are plotted in (**B**). (**C**) EPR spectra of membrane-bound endophilin reveals dimer interactions. Spectra were obtained either from protein that was fully labelled at position 227 (red trace) or from a mixture of 25% labelled protein and 75% unlabelled protein (black trace). The scan width was 200 Gauss. The amplitudes and line shapes of the respective spectra were very different owing to the strong dipolar spin–spin interactions that were present in the fully labelled case. The difference between the respective spectra was used to determine the distances using a Pake pattern analysis (Altenbach *et al*, 2001), and the blue spectrum can be used to evaluate the quality of this distance analysis. It is based on simulations in which the calculated distance distribution (shown in panel D) was used to generate a dipolar broadened spectrum from the black spectrum. This simulated spectrum closely corresponds to the observed spectrum for the fully labelled case indicating a good quality fit.

Figure 6 Endophilin has collaborative membrane binding and tubulation regions. (**A**) Table summarising constructs used, their liposome binding and tubulation abilities (see Materials and methods). N-BAR covers residues 1–247. The insert in helix1 is marked as H1I. F10E is a mutant of the hydrophobic face of the amphipathic helix. BAR covers residues 33–247. KKK-EEE is a mutant N-BAR with residues 171, 172 and 173 converted to glutamic acids. N-BAR ΔH1I is a deletion of residues 59–87 and insertion of two glycines. The other mutants are in H1I. BAR ΔH1I is residues 33–247 with the 59–87 deletion and two glycines inserted. Both the N-terminal amphipathic helix and BAR domain are required for efficient membrane binding of the N-BAR. Binding to 50 nm liposomes (p: pellet; s: supernatant) and tubulation of 200 or 400 nm liposomes (monitored by electron microscopy) are shown. In the binding assay, 50% of the pellet and 50% of the supernatant are loaded and % membrane binding was determined. The degree of tubulation is a reflection of the number of tubules. (**B**) Electron micrographs of liposome tubulation by rat endophilin-A1 N-BAR and mutants. Insets: Close-ups of the tubules show their similar morphology. The M70S+I71S mutant gives both wide and narrow tubules, some with budding profiles. (**C**) Table showing velocity ultracentrifugation results for mutants and WT protein. The N-BAR ΔH1I is a monomer as the apparent molecular weight is close to that of monomeric N-BAR domain (boxed). Both 40 and 150 μM protein were used and gave the same results. [1] Absorbance optics were used and the experiments were carried out at 20°C in 250 mM NaCl; [2] interference optics were used at 5°C in 150 mM NaCl and the remaining conditions as in Supplementary Figure 4B.

reduces both liposome binding and tubulation (Figure 6A and B). Both of these mutants lead to formation of non-uniform tubes and squashed liposomes (especially F10E, see arrows). Mutation of the positively charged lysine residues at the tips of the BAR domain to glutamates (KKK-EEE) also decreases binding and tubulation. Thus, both the N-terminal amphipathic helix and the BAR contribute to stable tubule formation.

A

Endophilin	Diagram	Membrane binding liposomes + − % binding	Tubules by EM
N-BAR		88	Very many
N-BAR F10E		52	Some
BAR		40	Few
N-BAR KKK-EEE		23	Very few
N-BAR ΔH1I		81	Some
N-BAR M70S, I71S		68	Many
N-BAR K76E, R78E		60	Very few
BAR ΔH1I		8	None

B

C

Endophilin	$S_{20,w}$ (Svedbergs)	$\bar{M}_{w,app}$ (kDa)
N-BAR[1]	2.83 ± 0.03	57.1 ± 2.2
N-BAR F10E[1]	3.19 ± 0.06	54.3 ± 2.5
N-BAR ΔH1I[2]	3.75 ± 0.2	25.4 ± 3.5
N-BAR M70S, I71S[2]	3.37 ± 0.05	59.3 ± 3.7
N-BAR K76E, R78E[2]	3.35 ± 0.05	56.5 ± 7.5

Three different mutants of the helix1 insert (H1I) were made: a deletion (N-BAR ΔH1I), a double mutant of hydrophobic residues (M70S, I71S) and a double mutant of positively charged residues (K76E, R78E). The N-BAR ΔH1I protein has the same overall secondary structure as WT protein according to CD spectroscopy (Supplementary Figure 3). It also binds liposomes similar to WT protein but tubulates less efficiently. This was surprising given that amphiphysin and arfaptin BAR domains do not have this helix1 insert and are good tubulators (Peter *et al*, 2004). However, when we tested this mutant by ultracentrifugation, we found that it was monomeric (Figure 6C and Supplementary Figure 4B). Hence for efficient curvature generation the spontaneous curvature driven by the amphipathic helix needs stabilization from the BAR domain dimer. It would also appear from the position of this insert in the structure that it may help to stabilise the dimer.

We further examined the role of the H1I with various point mutants. Binding to liposomes is decreased when the positive charges are made negative (K76E, R78E) and this mutant does not tubulate well. This is likely owing to the repulsion of the BAR from the similarly charged membrane. The M70S, I71S mutant is interesting because it binds well but gives rise to both narrow- (∼20 nm diameter) and WT-diameter tubules (although the narrow form are a minor component across the grids). We showed that M70 inserts into the membrane and thus this mutant is unlikely to allow the BAR domain to sit down on the membrane. The charge interaction of the BAR domain is still intact, as is the N-terminal amphipathic helix, and these narrow tubules are very similar to those made by the epsin ENTH domain, suggesting that this mutant results in an accumulation of helix insertion in the absence of the curvature-stabilising BAR domain. Both the M70S, I71S and the K76E, R78E double mutants form dimers (ultracentrifugation data) and thus these residues do not contribute significantly to dimer formation in solution. The N-BAR ΔH1I shows us that monomeric protein can bind to membranes but that promoting membrane curvature requires the dimerised BAR domain, as predicted from the structure. This is supported by the BAR ΔH1I binding weakly to all sizes of liposomes (Figure 6A and data not shown) and suggests that the curvature sensing we previously observed with the BAR domain is dependent on dimer formation. We propose that the H1I exhibits membrane interactions via insertion of an amphipathic helix. This is consistent with a role in defining the precise membrane curvature and does not exclude further interactions of H1I residues with integral membrane proteins.

Creation of high-curvature membranes promotes membrane fusion

The electron microscopy tubulation assay gives an accurate reflection of the morphological consequences that curvature proteins have on liposomes, but it is not quantitative, because tubules have a larger surface in contact with the grid than liposomes and thus these are over-represented, and protein-coated liposomes tend to bind better than naked liposomes. Importantly, by electron microscopy, we observe that the tubules formed are often longer than expected from tubulation of a single liposome (Figure 7A). We therefore tested whether the tubules fuse and if a fluorescence resonance energy transfer (FRET)-based membrane fusion assay would provide a more quantitative measurement (albeit indirect) of

the extent of tubulation. Phosphatidylserine liposomes were spiked with phosphatidylethanolamine lipids labelled on their polar headgroups with a FRET pair, NBD and rhodamine, and subsequently mixed with unlabelled liposomes (Struck *et al*, 1981). Concentrations of fluorophores are chosen such that FRET between them decreases on fusion with unlabelled liposomes (Struck *et al*, 1981). As a control, fusion can be initiated by addition of calcium (Figure 7B). Titration of the N-BAR domain into 50% labelled and 50% unlabelled liposomes (heterotypic case) decreases the FRET efficiency showing that fusion of the liposomes occurs (Figure 7C). There is a small background change resulting from the addition of protein, which is revealed if only the fluorescent liposomes are used (homotypic case, control). The BAR domain of endophilin tubulates inefficiently and does not lead to a decrease in FRET signal. We analysed all our mutants at 55 μM by calculating the ratio between the peaks in the emission spectrum (530 nm of NBD and 585 nm of rhodamine) to decrease systematic errors (Figure 7D). The background FRET change (likely owing to binding and immobilisation of the fluorophores) in the homotypic case is subtracted from the heterotypic case. More detailed results are shown in Supplementary Figure 5. We observe membrane fusion for the WT N-BAR domain, and M70S, I71S double mutant but not for the other mutants or the BAR domain on its own. This is consistent with the electron microscopy data and suggests that tubulation and fusion are coupled.

This *in vitro* observation raises the possibility that endophilin (and indeed other N-BAR proteins) *in vivo* may be fusogenic, although there is no direct evidence for this.

Model for endophilin membrane binding and curvature

Given the rigidity of the positively charged concave face of the BAR, this domain will act like a scaffold in binding to negatively charged membranes. We have previously shown that the BAR domain of endophilin binds better to liposomes of higher curvature (Gallop *et al*, 2005), which supports the idea that the endophilin BAR domain can scaffold membrane curvature using the crescent shape of the domain. We now confirm that the interaction of the BAR domain with membranes is electrostatic, as binding is sensitive to salt concentration (Figure 8A), as expected from the scaffolding hypothesis. Whereas the BAR domain alone does not bind to membranes in the presence of 250 mM NaCl, the N-BAR binds tightly. This is consistent with salt-insensitive interactions being provided by the amphipathic helix. Based on the observations with epsin1, where the amphipathic helix decreases the off-rate of membrane binding (Stahelin *et al*, 2003), we would predict that the amphipathic helices of endophilin would decrease the off-rate, anchoring the domain in the membrane. As electrostatic interactions act over a longer range than hydrophobic interactions, electrostatics are likely to be primary determinants of the on-rate and most of these charge interactions are contributed by the BAR domain (Zimmerberg and McLaughlin, 2004). This hypothesis is supported by the results in Figure 8B. If the N-BAR domain is pre-bound in physiological concentrations of salt, then addition of high salt (500 mM) leaves more protein bound than if the protein is added after high salt. (The liposomes remain intact during this experiment and sucrose-filled liposomes were also used to control for osmotic shock.) The displacement of the N-BAR domain bound to
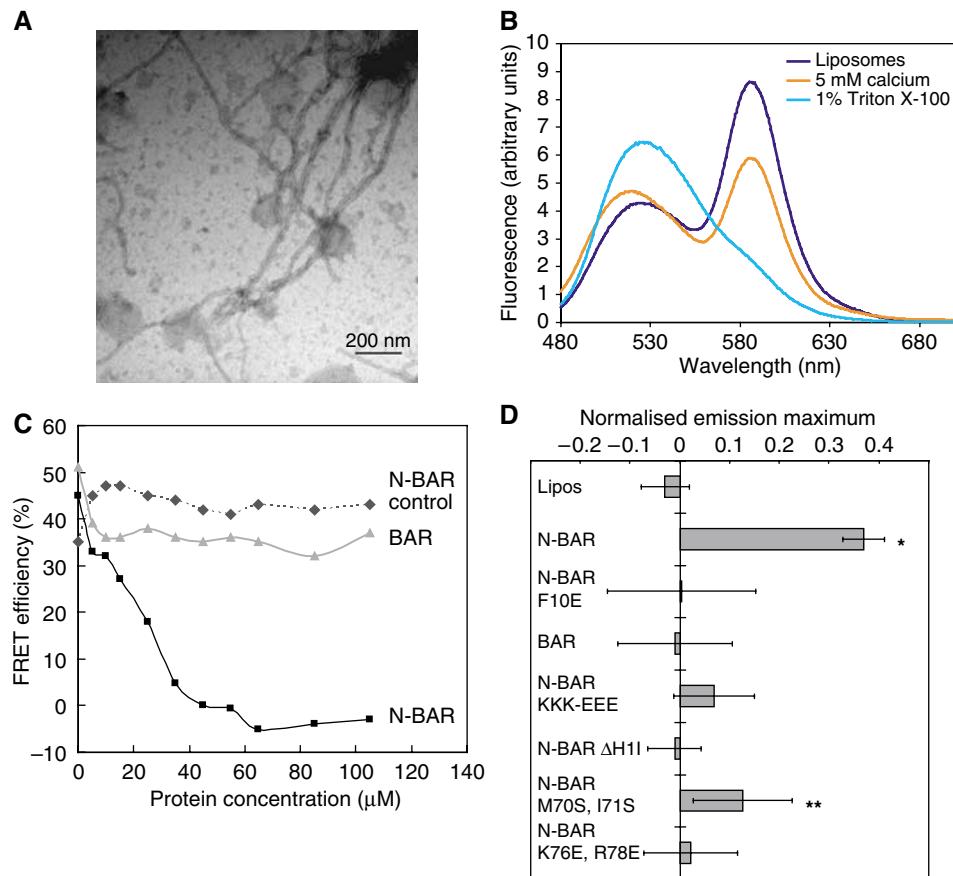
Figure 7 High membrane curvature promotes membrane fusion. (**A**) Example of endophilin N-BAR tubules made from liposomes extruded to a size cutoff of 400 nm. (**B**) Emission spectra from mixed liposomes in the absence and presence of calcium (which promotes fusion) and Triton (to obtain total donor fluorescence). See Materials and methods for details of the assay. (**C**) FRET assay of membrane fusion, showing dilution of the FRET pair into unlabelled liposome in the presence of the N-BAR (see Results). The N-BAR control has no unlabelled liposomes and thus there can be no dilution of the FRET pair. The BAR domain does not lead to membrane fusion. As highly curved membranes are more fusogenic, we believe that the fusion seen with the N-BAR domain is a readout of the efficiency of curvature generation. (**D**) Comparison of mutants and WT N-BAR domains at 55 μM in the fusion assay. Values displayed in the bar chart ± s.e.m. are the difference in the ratios of emission maxima between experiment (mixed liposomes (530/585 nm)) and controls (uniformly labelled liposomes (530/585 nm)) (see Results). Student's *t*-test *$P < 0.001$, **$P < 0.2$.

membranes is less vulnerable to the charge screening effect of ionic strength than is *de novo* binding of the domain. The charge contribution is mostly from the BAR domain, which also binds better to small liposomes (Gallop *et al*, 2005). The preference for smaller liposomes is evident in this assay: when salt is added before protein, more protein is bound to the 50 nm liposomes than to the 400 nm ones. This leads to the hypothesis that as well as acting to generate curvature via the amphipathic helices and BAR domain scaffold, N-BAR domains can also respond to membrane curvature, as binding to areas of high membrane curvature is kinetically favoured. This gives a positive feedback loop between curvature sensing and generation, leading to very rapid membrane deformation.

To summarise, there are two synergistic ways by which endophilin modulates membrane curvature (Figure 8C). The penetration of the amphipathic helices leads to an asymmetry between the outer and inner leaflets of the bilayer causing an increase in positive curvature whereas the concave face of the BAR domain acts to scaffold membrane curvature. In Figure 8C, we show the amphipathic helices under the BAR domain, where it could shield the negatively charged patch on this surface and position the helices. This would correlate well with the immobilisation of some of these residues in EPR spectra. The internal amphipathic helix stabilises the formed dimer as well as further promoting membrane curvature generation. The principles described here for amphipathic helix insertion and BAR domain dimerisation and binding are expected to hold for all N-BAR domains. In Figure 8D, we propose a temporal model by which these processes occur.

Discussion

Here we have demonstrated directly the folding of an amphipathic helix and its insertion into membranes for the N-terminus of endophilin N-BAR. We determined its orientation in the membrane and penetration depth. The EPR technique also allowed us to show that the BAR domain dimer is present on the membrane. Using the monomeric ΔH1I protein, we can also conclude that dimerisation is essential for the action of the BAR domain but that some binding and membrane deformation can be provided by the
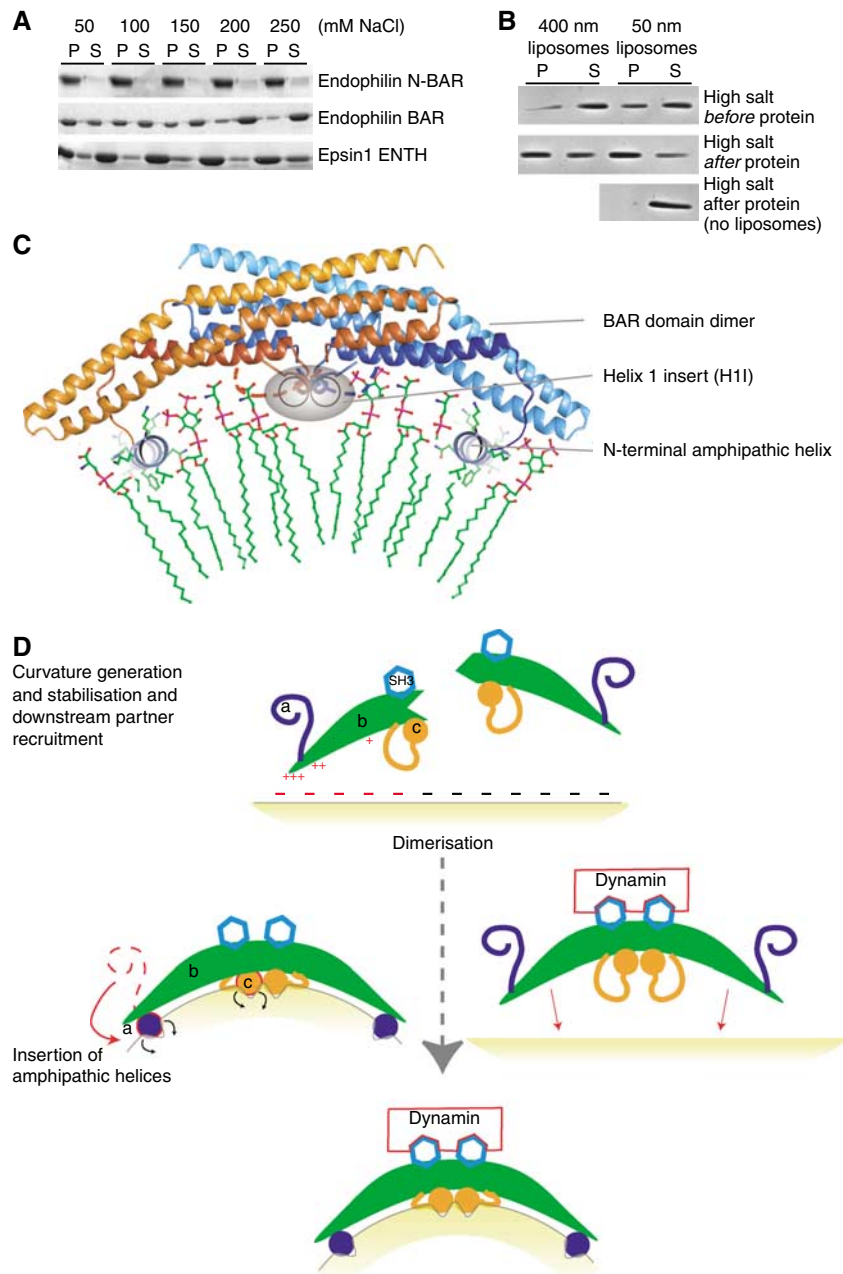
Figure 8 Endophilin N-BAR domain binding to membrane is initially driven by electrostatics. (**A**) Salt sensitivity of the BAR domain shows the predominance of electrostatics in the interaction. Like the N-BAR domain of endophilin, the epsin ENTH domain inserts an amphipathic helix giving a hydrophobic contribution to the interaction. Liposomes were sedimented and pellets (p) and supernatants (s) were separated by SDS–PAGE. (**B**) Recruitment of N-BAR domain to liposomes is driven by electrostatics, but after the initial interaction the dissociation is not salt-sensitive. In the 'salt before' experiment, protein was incubated with liposomes in the presence of 500 mM NaCl for 10 min. In the 'salt after' experiment, 500 mM NaCl was added to the protein liposome mix after the 10 min incubation and further incubated for 3 min. (**C**) Endophilin N-BAR domain binding to membranes. From experiments in Figures 3 and 5 we know that the BAR binds via its concave surface and from Figure 2 we know that the N-terminal amphipathic helix lies flat in the plane of the membrane and the depth of insertion, but we do not have any information on the orientation of the N-terminal amphipathic helix in the membrane with respect to the BAR. We know the position of the first turn of the additional amphipathic helix insert in helix1 and the membrane insertion of M70 and have drawn the remainder of this insert as a dashed line. If amphipathic helices are parallel to the long axis of the BAR, then the domain will favour two-dimensional membrane curvature. If the helices are perpendicular, then the domain will favour one-dimensional curvature. (**D**) Hypothetical model of the stages of endophilin N-BAR membrane binding. The N-BAR domain of endophilin is made of three parts, (a) an N-terminal amphipathic helix, (b) a BAR monomer and (c) an internal amphipathic helix and additional loop sequences. Monomeric proteins are attracted to negatively charged membranes. Insertion of amphipathic helices (both N-terminal and internal helices) promotes curvature, and at the same time dimerisation of the BAR stabilises the protein on the membrane. Once curvature is initiated, the energetic barriers for further N-BAR domain recruitment will be lower, resulting in a scaffolding of the curvature. Given the presentation of two SH3 domains per dimer on the membrane, multimeric ligands will interact with higher avidity than to the monomeric proteins in the cytosol. Thus, N-BAR proteins recruit ligands to areas of high membrane curvature. It is likely that membrane specificity is also encoded within this domain, in particular the amphipathic helices would be well positioned to interact with membrane proteins, and indeed there are additional resides in the helix 1 insert not included in the amphipathic helix which have no known function and may be important for specificity. It can also be noted that this insert sequence can differ significantly between endophilin family members and also between the endophilins and nadrins.

amphipathic helix in the absence of the dimerised BAR domain scaffold. A similar conclusion can be drawn from the N125 construct used previously (Farsad *et al*, 2001) where we would posit that the tubulation observed is owing to the insertion of the amphipathic helices rather than the BAR. The importance of the N-terminal amphipathic helix to endophilin function *in vivo* was demonstrated in *C. elegans* where F10E endophilin did not rescue the endophilin-null mutant (Schuske *et al*, 2003).

We propose that a major component of any budding pathway is a mechanism for bending membranes to the desired curvature. In clathrin-coated vesicle formation, epsin molecules can bind to PtdIns(4,5)P$_2$ and insert an amphipathic helix promoting membrane curvature while at the same time stimulating clathrin polymerisation and thus stabilisation of the generated curvature (Ford *et al*, 2002). It may well be that active insertion of an amphipathic helix is a general mechanism in budding of many types of vesicles, and this role can be executed for example by other ENTH domain proteins or by small GTPases of the Arf and Arl families. Many BAR domain proteins also have associated amphipathic helices (either in *cis*: N-BAR proteins; or in *trans*: e.g. Arf binding to arfaptin) and thus we would predict that these are adept at effecting membrane curvature. We have shown that electrostatics seem to govern the on-rate of the N-BAR domain on membranes, whereas the interactions of amphipathic helices with membranes seem to limit the off-rate. It is interesting that the endophilin dimer will have four amphipathic helix insertions and thus this protein is likely to reside for a considerable period on highly curved membranes. The N-terminal amphipathic helix has the midpoint of its insertion at the phosphate level of headgroups, thus acting as a wedge in the membrane at the same time as anchoring itself via positive charges to negatively charged lipid headgroups.

It is interesting to consider that N-BAR domains may lead to a positive feedback loop whereby curvature generation leads to further curvature generation allowing very rapid invagination once a critical concentration of endophilin is reached on the membrane. Also, the minimal radius of curvature is likely to be defined by the dimensions of the BAR domain, as shown by tubulation and vesiculation in our electron microscopy observations. Thus, when the concave face is disrupted, as in the M70S, I71S mutant, narrower tubule widths can be observed.

We observe many tubules *in vitro* after N-BAR domain binding to liposomes, and *in vivo* tubulation of membrane compartments is also observed on overexpression of various N-BAR domains (Razzaq *et al*, 2001; Lee *et al*, 2002; data not shown). In *Drosophila* muscle, the N-BAR-containing protein amphiphysin lines the muscle T-tubule network and is involved in its stabilisation (Razzaq *et al*, 2001). However, *Drosophila* amphiphysin does not bind to dynamin and thus these tubular structures are not severed, whereas in vesicle budding the recruitment of dynamin by the SH3 domains of N-BAR proteins will likely result in vesicle scission rather than extensive tubulation. Thus, the balance between tubulation and vesiculation may depend largely on the recruitment of downstream interaction partners.

The binding of downstream partners may also be regulated by the dimerisation of the proteins on membranes. We have measured the affinity of amphiphysin SH3 domain for dyna-min interaction peptides as 50–100 μM. This is a very weak interaction. However, as dynamin is a dimer, multiple amphiphysin SH3 domains bound to beads can be used to purify dynamin (Wigge *et al*, 1997). Likewise, it is very likely that endophilin membrane-bound dimers will have a much greater avidity for dynamin than endophilin monomers in solution and thus recruit dynamin to areas of high membrane curvature.

We had previously observed that the tubules formed by epsin, amphiphysin and others were longer than would be expected from the initial liposome size. We show here that on addition of curvature-generating endophilin N-BAR domain, membrane fusion takes place. This has provided a complementary approach to electron microscopy as a more quantitative readout of the action of mutants on liposome deformation. More interestingly, it raises the possibility that exocytosis or other vesicle fusion events can be enhanced by increased curvature generation.

Overexpression of endophilin A1 (without its SH3 domain) in fibroblasts does not affect the endocytosis of transferrin (a clathrin-mediated pathway), but overexpression of a similar construct of amphiphysin does (data not shown). This is probably owing to targeting sequences in amphiphysin, which allow it to bind to both clathrin and adaptors, which are absent in endophilin. The absence of these interaction sequences makes endophilin distinct from clathrin-endocytic proteins. It has previously been noted that endophilin appears to be transported to synapses on vesicles (Pierrat *et al*, 2001) (and thus is likely to be on synaptic vesicles before fusion), binds the membrane scission protein dynamin and is missing the targeting sequences for recruitment into clathrin-coated pits. We therefore speculate that the role of endophilin is distinct from that of amphiphysin, and that the role of endophilin is to generate/stabilise curvature in a clathrin-independent mechanism in synapses, where it is found enriched.

Given that endophilin is enriched in synapses, is capable of curvature-induced curvature generation, binds to dynamin and may well be targeted to synapses on vesicles, this may suggest a possible involvement in fast, 'kiss-and-run' clathrin-independent endocytosis at synapses. This is consistent with the observations of Schwarz and co-workers (Dickman *et al*, 2005) in endophilin-null mutants, where the kinetics of the remaining endocytosis is slow. An inhibition of fast, kiss-and-run endocytosis would lead to a kinetic slowing in synaptic vesicle endocytosis, as observed in multiple systems, as the time constant for the clathrin-mediated pathway is slow (Jockusch *et al*, 2005). We note that the previous assignment of endophilin to clathrin-mediated endocytosis (Ringstad *et al*, 1999; Verstreken *et al*, 2002) is without firm molecular basis and that the observed accumulation of clathrin-coated intermediates after endophilin depletion could equally be due to a compensatory upregulation in this pathway as opposed to its inhibition.

In this paper, we have presented a molecular mechanism of how the BAR and amphipathic helices of N-BAR domains work as a unit to promote membrane curvature. As membrane-bound protein is dimeric, it will lead to the presentation of two SH3 domains, favouring binding to multimeric ligands (such as dynamin). Thus, a low-affinity dimerisation of the N-BAR domain may be a mechanism not only to regulate the recruitment of endophilin to membranes but

also to regulate binding partner recruitment to areas of high membrane curvature.

Materials and methods

Constructs and liposome assays

GST full-length rat endophilin, GST rat endophilin N-BAR domain (residues 1–247) and GST-human arfaptin2 BAR domain (residues 117–end) were cloned into ER1/Not1 sites of pGex4T2 and proteins were thrombin cleaved before purification by anion exchange and gel filtration. Rat synaptojanin 145 (gift from Peter Parker) was cloned into the Not1 site of pBac4x1 with a hexa-histidine tag at the C-terminus. Protein was purified on Ni-NTA agarose (Qiagen) followed by S200 gel filtration. Folch Fraction I (Sigma) liposomes in 150 mM NaCl and 20 mM HEPES (pH 7.4) were extruded 11 times through polycarbonate membranes (Avanti) to achieve desired diameter. For tubulation assays, typically 1 mg/ml 200 nm liposomes were incubated for 10 min with 10, 20 and 40 μM protein. Samples were spread on electron microscopy grids and stained using 5% uranyl acetate. For details, see http://www.endocytosis. org/techniqs/techniqs.htm. For salt sensitivity experiments, the endophilin N-BAR domain was bound at a concentration of 6 μM to Folch liposomes at a concentration of 0.6 mg/ml. The 'salt after' samples were diluted to a concentration of 175 mM NaCl before ultracentrifugation, which separates out the liposomes (which pellet). For the 'salt before' samples, dilution was performed after ultracentrifugation. Other methods not listed are found in Supplementary data.

References

Altenbach C, Greenhalgh DA, Khorana HG, Hubbell WL (1994) A collision gradient method to determine the immersion depth of nitroxides in lipid bilayers: application to spin-labeled mutants of bacteriorhodopsin. *Proc Natl Acad Sci USA* **91:** 1667–1671

Altenbach C, Oh KJ, Trabanino RJ, Hideg K, Hubbell WL (2001) Estimation of inter-residue distances in spin labeled proteins at physiological temperatures: experimental strategies and practical limitations. *Biochemistry* **40:** 15471–15482

Bauerfeind R, Takei K, De Camilli P (1997) Amphiphysin I is associated with coated endocytic intermediates and undergoes stimulation-dependent dephosphorylation in nerve terminals. *J Biol Chem* **272:** 30984–30992

Chen Y, Deng L, Maeno-Hikichi Y, Lai M, Chang S, Chen G, Zhang JF (2003) Formation of an endophilin-Ca²⁺ channel complex is critical for clathrin-mediated synaptic vesicle endocytosis. *Cell* **115:** 37–48

Cremona O, Di Paolo G, Wenk MR, Luthi A, Kim WT, Takei K, Daniell L, Nemoto Y, Shears SB, Flavell RA, McCormick DA, De Camilli P (1999) Essential role of phosphoinositide metabolism in synaptic vesicle recycling. *Cell* **99:** 179–188

Dickman DK, Horne JA, Meinertzhagen IA, Schwarz TL (2005) A slowed classical pathway rather than kiss-and-run mediates endocytosis at synapses lacking synaptojanin and endophilin. *Cell* **123:** 521–533

Evergren E, Marcucci M, Tomilin N, Low P, Slepnev V, Andersson F, Gad H, Brodin L, De Camilli P, Shupliakov O (2004) Amphiphysin is a component of clathrin coats formed during synaptic vesicle recycling at the lamprey giant synapse. *Traffic* **5:** 514–528

Farsad K, Ringstad N, Takei K, Floyd SR, Rose K, De Camilli P (2001) Generation of high curvature membranes mediated by direct endophilin bilayer interactions. *J Cell Biol* **155:** 193–200

Ford MG, Mills IG, Peter BJ, Vallis Y, Praefcke GJ, Evans PR, McMahon HT (2002) Curvature of clathrin-coated pits driven by epsin. *Nature* **419:** 361–366

Ford MG, Pearse BM, Higgins MK, Vallis Y, Owen DJ, Gibson A, Hopkins CR, Evans PR, McMahon HT (2001) Simultaneous binding of PtdIns(4,5)P2 and clathrin by AP180 in the nucleation of clathrin lattices on membranes. *Science* **291:** 1051–1055

Gad H, Ringstad N, Low P, Kjaerulff O, Gustafsson J, Wenk M, Di Paolo G, Nemoto Y, Crun J, Ellisman MH, De Camilli P, Shupliakov O, Brodin L (2000) Fission and uncoating of synaptic clathrin-coated vesicles are perturbed by disruption of interactions with the SH3 domain of endophilin. *Neuron* **27:** 301–312

Gallop JL, Butler PJG, McMahon HT (2005) Endophilin and CtBP/BARS are not acyl transferases in endocytosis or Golgi fission. *Nature* **438:** 675–678

Guichet A, Wucherpfennig T, Dudu V, Etter S, Wilsch-Brauniger M, Hellwig A, Gonzalez-Gaitan M, Huttner WB, Schmidt AA (2002) Essential role of endophilin A in synaptic vesicle budding at the *Drosophila* neuromuscular junction. *EMBO J* **21:** 1661–1672

Huttner WB, Schmidt A (2000) Lipids, lipid modification and lipid–protein interaction in membrane budding and fission—insights from the roles of endophilin A1 and synaptophysin in synaptic vesicle endocytosis. *Curr Opin Neurobiol* **10:** 543–551

Jockusch WJ, Praefcke GJK, McMahon HT, Lagnado L (2005) Clathrin-dependent and clathrin-independent retrieval of synaptic vesicles in retinal bipolar cells. *Neuron* **46:** 1–10

Lee E, Marcucci M, Daniell L, Pypaert M, Weisz OA, Ochoa GC, Farsad K, Wenk MR, De Camilli P (2002) Amphiphysin 2 (Bin1) and T-tubule biogenesis in muscle. *Science* **297:** 1193–1196

Lee MC, Orci L, Hamamoto S, Futai E, Ravazzola M, Schekman R (2005) Sar1p N-terminal helix initiates membrane curvature and completes the fission of a COPII vesicle. *Cell* **122:** 605–617

McMahon HT, Gallop JL (2005) Membrane curvature and mechanisms of dynamic cell membrane remodelling. *Nature* **428:** 590–596

Peter BJ, Kent HM, Mills IG, Vallis Y, Butler PJ, Evans PR, McMahon HT (2004) BAR domains as sensors of membrane curvature: the amphiphysin BAR structure. *Science* **303:** 495–499

Pierrat B, Simonen M, Cueto M, Mestan J, Ferrigno P, Heim J (2001) SH3GLB, a new endophilin-related protein family featuring an SH3 domain. *Genomics* **71:** 222–234

Rabenstein MD, Shin YK (1995) Determination of the distance between two spin labels attached to a macromolecule. *Proc Natl Acad Sci USA* **92:** 8239–8243

Razzaq A, Robinson IM, McMahon HT, Skepper JN, Su Y, Zelhof AC, Jackson AP, Gay NJ, O'Kane CJ (2001) Amphiphysin is necessary for organization of the excitation–contraction coupling machinery of muscles, but not for synaptic vesicle endocytosis in *Drosophila*. *Genes Dev* **15:** 2967–2979

Rikhy R, Kumar V, Mittal R, Krishnan KS (2002) Endophilin is critically required for synapse formation and function in *Drosophila melanogaster*. *J Neurosci* **22:** 7478–7484

Ringstad N, Gad H, Low P, Di Paolo G, Brodin L, Shupliakov O, De Camilli P (1999) Endophilin/SH3p4 is required for the transition from early to late stages in clathrin-mediated synaptic vesicle endocytosis. *Neuron* **24:** 143–154

Schuske KR, Richmond JE, Matthies DS, Davis WS, Runz S, Rube DA, van der Bliek AM, Jorgensen EM (2003) Endophilin is required for synaptic vesicle endocytosis by localizing synaptojanin. *Neuron* **40:** 749–762

Simpson F, Hussain NK, Qualmann B, Kelly RB, Kay BK, McPherson PS, Schmid SL (1999) SH3-domain-containing proteins function at distinct steps in clathrin-coated vesicle formation. *Nat Cell Biol* **1:** 119–124

Stahelin RV, Long F, Peter BJ, Murray D, De Camilli P, McMahon HT, Cho W (2003) Contrasting membrane interaction mechanisms of AP180 N-terminal homology (ANTH) and epsin N-terminal homology (ENTH) domains. *J Biol Chem* **278:** 28993–28999

Struck DK, Hoekstra D, Pagano RE (1981) Use of resonance energy transfer to monitor membrane fusion. *Biochemistry* **20:** 4093–4099

Verstreken P, Kjaerulff O, Lloyd TE, Atkinson R, Zhou Y, Meinertzhagen IA, Bellen HJ (2002) Endophilin mutations block clathrin-mediated endocytosis but not neurotransmitter release. *Cell* **109:** 101–112

Weissenhorn W (2005) Crystal structure of the endophilin-A1 BAR domain. *J Mol Biol* **351:** 653–661

Wigge P, Kohler K, Vallis Y, Doyle CA, Owen D, Hunt SP, McMahon HT (1997) Amphiphysin heterodimers: potential role in clathrin-mediated endocytosis. *Mol Biol Cell* **8:** 2003–2015

Zimmerberg J, McLaughlin S (2004) Membrane curvature: how BAR domains bend bilayers. *Curr Biol* **14:** R250–R252